Increased thermogenesis by a noncanonical pathway in ANGPTL3/8-deficient mice

Serena Banfi[a,b], Viktoria Gusarova[c], Jesper Gromada[c], Jonathan C. Cohen[b,1], and Helen H. Hobbs[a,b,d,1]

[a]Department of Molecular Genetics, University of Texas Southwestern Medical Center, Dallas, TX 75390; [b]Department of Internal Medicine, University of Texas Southwestern Medical Center, Dallas, TX 75390; [c]Regeneron Pharmaceuticals, Inc., Tarrytown, NY 10591; and [d]The Howard Hughes Medical Institute, University of Texas Southwestern Medical Center, Dallas, TX 75390

Contributed by Helen H. Hobbs, December 21, 2017 (sent for review October 6, 2017; reviewed by Alan D. Attie, Sheila Collins, Ira J. Goldberg, and Rudolf Zechner)

Dietary triglyceride (TG) is the most efficient energy substrate. It is processed and stored at substantially lower metabolic cost than is protein or carbohydrate. In fed animals, circulating TGs are preferentially routed for storage to white adipose tissue (WAT) by angiopoietin-like proteins 3 (A3) and 8 (A8). Here, we show that mice lacking A3 and A8 ($A3^{-/-}A8^{-/-}$ mice) have decreased fat mass and a striking increase in temperature (+1 °C) in the fed (but not fasted) state, without alterations in food intake or physical activity. Subcutaneous WAT (WAT-SQ) from these animals had morphologic and metabolic changes characteristic of beiging. O_2 consumption rates (OCRs) and expression of genes involved in both fatty acid synthesis and fatty acid oxidation were increased in WAT-SQ of $A3^{-/-}A8^{-/-}$ mice, but not in their epididymal or brown adipose tissue (BAT). The hyperthermic response to feeding was blocked by maintaining $A3^{-/-}A8^{-/-}$ mice at thermoneutrality or by treating with a β3-adrenergic receptor (AR) antagonist. To determine if sympathetic stimulation was sufficient to increase body temperature in $A3^{-/-}A8^{-/-}$ mice, WT and $A3^{-/-}A8^{-/-}$ animals were maintained at thermoneutrality and then treated with a β3-AR agonist; treatment induced hyperthermia in $A3^{-/-}A8^{-/-}$, but not WT, mice. Antibody-mediated inactivation of both circulating A3 and A8 induced hyperthermia in WT mice. Together, these data indicate that A3 and A8 are essential for efficient storage of dietary TG and that disruption of these genes increases feeding-induced thermogenesis and energy utilization.

ANGPTL3 | ANGPTL8 | adipose tissue | hyperthermia

Circulating triglycerides (TGs) are partitioned between oxidative tissues and white adipose tissue (WAT) by lipoprotein lipase (LPL), an enzyme located on capillary endothelia. LPL releases fatty acids (FAs) from TGs in circulating lipoproteins for uptake by underlying tissues. The activity of LPL in different tissue beds is regulated in response to nutritional cues. In fasted animals, LPL activity is high in oxidative tissues and low in WAT, thus favoring the uptake of circulating TG by oxidative tissues (1, 2). Feeding decreases LPL activity in oxidative tissues and increases the activity of the enzyme in WAT, thus replenishing WAT energy stores by increasing FA uptake.

The changes in LPL activity associated with fasting and refeeding are coordinated by secreted proteins of the angiopoietin-like protein (ANGPTL) family: ANGPTL3 (A3), ANGPTL4 (A4), and ANGPTL8 (A8). All three proteins inhibit LPL activity, but A4 is increased by fasting and acts locally in WAT (3), whereas A8 is stimulated by feeding (4–6) and acts together with A3 to inhibit LPL via the systemic circulation (6). Consequently, in fasted animals, A4 powerfully suppresses LPL activity in WAT, directly suppressing uptake of FAs from circulating lipoproteins (2). The very low expression of A8 during fasting limits systemic inhibition of LPL activity by the A3/A8 complex, resulting in high LPL activity in oxidative tissues (6–8). Upon refeeding, A4 expression is decreased in WAT, leading to increased LPL activity and TG-FA uptake in that organ (2). Conversely, feeding strongly stimulates A8 expression, promoting the formation of A3/A8 complexes in the circulation and thus systemic inhibition of LPL activity and TG-FA uptake in oxidative tissues (6, 8–10).

In addition to the striking effects of A3 and A8 on circulating lipoprotein metabolism, both proteins appear to be required for normal energy substrate selection. Mice lacking A3 ($A3^{-/-}$ mice) or A8 ($A8^{-/-}$ mice) fail to increase very low-density lipoprotein (VLDL)-TG uptake into WAT after feeding (7, 9). In $A3^{-/-}$ mice, we previously showed that the decrease in VLDL-TG uptake is compensated by increased uptake of glucose and de novo synthesis of FAs in WAT (9). Thus, WAT stores are largely preserved in $A3^{-/-}$ mice (9). In mice lacking A8, a similar reduction in postprandial VLDL-TG uptake is observed (8). However, in these animals, the compensatory mechanism(s) are insufficient to maintain WAT stores of TG, and they accrete substantially less WAT than do their wild-type (WT) littermates (8).

These differences in the phenotypes of $A3^{-/-}$ and $A8^{-/-}$ mice indicate that the two proteins have distinct functions. Here, we show that targeted inactivation of *Angptl8* (*A8*) in mice results in a hypermetabolic phenotype that is exacerbated by joint inactivation of *Angptl3* (*A3*). Double-knockout (double-KO) mice ($A3^{-/-}A8^{-/-}$ mice) fed ad libitum have increased body temperatures and oxygen (O_2) consumption, which can be normalized by prolonged (14 h) fasting or β-adrenergic receptor (AR) blockade. No changes were observed in the morphology, mitochondrial content, or O_2 consumption of epididymal WAT (WAT-Epi) or brown adipose tissue (BAT) in the $A3^{-/-}A8^{-/-}$

Significance

White adipose tissue (WAT) serves as an energy reservoir during fasting and is replenished with fatty acids from circulating triglycerides upon refeeding. We showed previously that postprandial partitioning of fatty acids between oxidative and storage tissues is mediated by angiopoietin-like proteins 3 (A3) and 8 (A8). Here, we show that disruption of both *Angptl3* and *Angptl8* in mice causes striking alterations in energy metabolism: reduced fat mass, hyperthermia, increased metabolic rate, and beiging of subcutaneous WAT. The hypermetabolic features of the $A3^{-/-}A8^{-/-}$ mice were most pronounced in fed animals, and attenuated with fasting and β3-adrenergic receptor blockade. These data indicate that A3 and A8 promote efficient energy utilization by tissues and limit the increase in energy expenditure associated with food intake.

Author contributions: S.B., J.C.C., and H.H.H. designed research; S.B. performed research; V.G. and J.G. contributed new reagents/analytic tools; S.B., V.G., J.G., J.C.C., and H.H.H. analyzed data; and S.B., V.G., J.G., J.C.C., and H.H.H. wrote the paper.

Reviewers: A.D.A., University of Wisconsin–Madison; S.C., Sanford Burnham Medical Research Institute at Lake Nona; I.J.G., New York University Medical Center; and R.Z., University of Graz.

Conflict of interest statement: V.G. and J.G. are employees and shareholders of Regeneron Pharmaceuticals, Inc. J.C.C. is a paid consultant for Regeneron on a different project.

[1]To whom correspondence may be addressed. Email: jonathan.cohen@utsouthwestern.edu or helen.hobbs@utsouthwestern.edu.

This article contains supporting information online at www.pnas.org/lookup/suppl/doi:10.1073/pnas.1717420115/-/DCSupplemental.

mice, but their subcutaneous WAT (WAT-SQ) showed features characteristic of beiging (11), including reduced adipocyte size and increased mitochondrial mass and O_2 uptake. Together, our data support a model in which A3 and A8 promote efficient energy utilization by coordinating the allocation of circulating TG among tissues in accordance with their nutritional needs and by limiting β-AR–stimulated increases in energy consumption during the postprandial period.

Results

***A3*$^{-/-}$*A8*$^{-/-}$ Mice Have Reduced Fat Mass and Lean Body Mass.** All mice used in this study were back-crossed onto a C57BL/6J background (N6) to minimize genetic differences unrelated to the targeted genes. *A3*$^{-/-}$ mice were born in the expected Mendelian ratios (Tables S1 and S2), but *A8*$^{-/-}$ and *A3*$^{-/-}$*A8*$^{-/-}$ double-KO mice were born at lower than expected frequency (Tables S3–S6). Only 9% of the offspring of *A8*$^{+/-}$ × *A8*$^{+/-}$ crosses were homozygous for the mutant *A8* allele. Among offspring of doubly heterozygous mice, *A3*$^{-/-}$*A8*$^{-/-}$ offspring were observed at less than half the expected frequency (2.5% observed vs. 6.25% expected). The dearth of *A3*$^{-/-}$*A8*$^{-/-}$ mice was accounted for by the inactivation of *A8*. Only 9% of the offspring of doubly heterozygous mice were homozygous for the mutant *A8* allele, whereas the fraction of *A3*$^{-/-}$ mice (18%) was consistent with expectation (22%). No differences in fertility were seen in the offspring of *A3*$^{-/-}$*A8*$^{-/-}$ and WT mice (average litter sizes $n = 4.4$ and $n = 4.3$, respectively).

Consistent with prior studies, body weight and fat content were similar in *A3*$^{-/-}$ male mice (9) and reduced in *A8*$^{-/-}$ mice (8) compared with their WT littermates (Fig. 1 *A* and *B*, respectively). By 6 wk of age, chow-fed *A8*$^{-/-}$ and *A3*$^{-/-}$*A8*$^{-/-}$ mice weighed significantly less than WT animals (Fig. 1*A*), although the weights of WT and *A3*$^{-/-}$*A8*$^{-/-}$ were similar at birth (Fig. S1*A*). The differences in weight were maintained until at least 16 wk of age and were due primarily to a decrease in fat mass, although lean body mass was also lower in the male double-KO animals (Fig. 1*B*). The changes in body weight and fat mass were attenuated in female *A8*$^{-/-}$ mice (Fig. S1*B*), but were significantly lower in the female *A3*$^{-/-}$*A8*$^{-/-}$ mice compared with littermate controls.

***A3*$^{-/-}$*A8*$^{-/-}$ Mice Are Hypermetabolic.** To define the metabolic basis for the decreased fat mass in *A8*$^{-/-}$ and *A3*$^{-/-}$*A8*$^{-/-}$ mice, we placed mice in metabolic cages and monitored their food intake, VO_2 consumption, VCO_2 output, and physical activity. No differences in food intake or physical activity were observed among the male or female mouse lines (Fig. 1*C* and Fig. S1*C*). VO_2 was higher in male ($P < 0.05$), but not female, *A8*$^{-/-}$ mice (Fig. 1*D* and Fig. S1 *D*, *Upper*), and both VO_2 consumption and VCO_2 output were increased in the male and female *A3*$^{-/-}$*A8*$^{-/-}$ mice ($P < 0.001$) (Fig. 1*D* and Fig. S1*D*). The increases in VO_2 consumption and VCO_2 output of the *A3*$^{-/-}$*A8*$^{-/-}$ mice were apparent in both the light and dark phases of the diurnal cycle (Fig. S2). The respiratory exchange ratio (RER) increased at night and decreased during the day, as expected, but no differences in RER were observed among the strains (Fig. S3).

***A3*$^{-/-}$*A8*$^{-/-}$ Mice Have Increased Body Temperature in the Fed, but Not Fasted, State.** Among male mice, rectal temperatures were consistently higher in the three KO lines than in the WT animals, although the increase was most pronounced in the *A3*$^{-/-}$*A8*$^{-/-}$ mice (Fig. 2 *A*, *Left*). Female *A8*$^{-/-}$ and *A3*$^{-/-}$*A8*$^{-/-}$ mice had significantly higher rectal temperatures, but the temperatures of the female *A3*$^{-/-}$ mice did not differ from those of control animals (Fig. 2 *A*, *Right*).

Since expression of A3, and especially A8, is increased with feeding, we examined the effect of food intake on temperature in the *A3*$^{-/-}$*A8*$^{-/-}$ mice. The rectal temperatures of mice kept in metabolic cages through the fasting/refeeding cycle are shown in Fig. 2*B*. In this experiment, mice were allowed to acclimate to the cages for 2 d with ad libitum access to food. On the third day, VO_2 consumption and VCO_2 output were measured, and rectal temperatures were taken. As noted above, rectal temperatures were significantly higher in *A3*$^{-/-}$*A8*$^{-/-}$ mice than in WT mice under ad libitum feeding conditions (Fig. 2 *B*, *Upper*). Food was then withdrawn for 24 h, and the temperature measurements were repeated (middle time point). Food deprivation for 24 h reduced body temperatures in both lines and abolished the differences observed in WT and KO animals fed ad libitum. Food was then restored, and a third set of temperature measurements

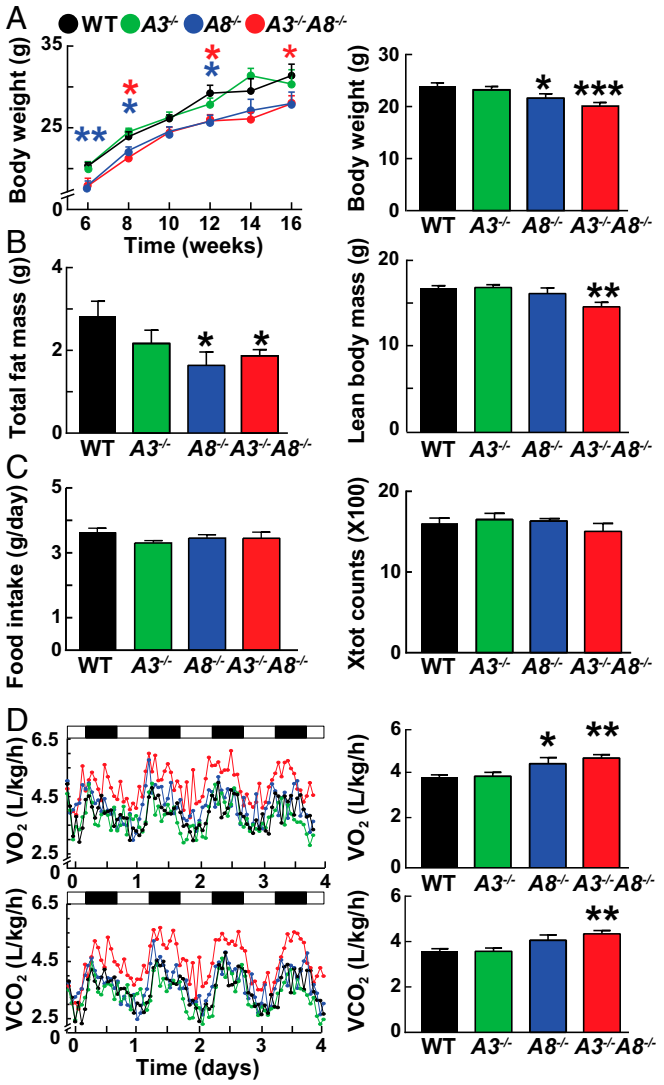

Fig. 1. Metabolic characterization of *A3*$^{-/-}$, *A8*$^{-/-}$, *A3*$^{-/-}$*A8*$^{-/-}$, and WT male mice. (*A*) Body weights of *A3*$^{-/-}$, *A8*$^{-/-}$, *A3*$^{-/-}$*A8*$^{-/-}$, and WT mice (n = 10–12 per group) were measured every other week starting at 6 wk of age (*Right*). Body weight (*A*) and composition (*B*) were measured in mice aged 8–10 wk ($n = 6$ per group). The experiment was repeated once, and the results were similar. (*C*) Food intake (*Left*) and total activity (*Right*) were assessed in mice housed individually in metabolic cages for 7 d. (*D*) Both O_2 consumption and CO_2 output were measured for 1 min at 30-min intervals for four consecutive days while the mice were housed in metabolic cages ($n = 9$; age 8–12 wk). Values are means ± SEM. Group means for VO_2 consumption and VCO_2 output were compared by ANCOVA with body weight as a covariate; similar results were obtained with an unpaired *t* test. Group means for other parameters were compared by using unpaired *t* tests. *$P < 0.05$; **$P < 0.01$; ***$P < 0.001$.

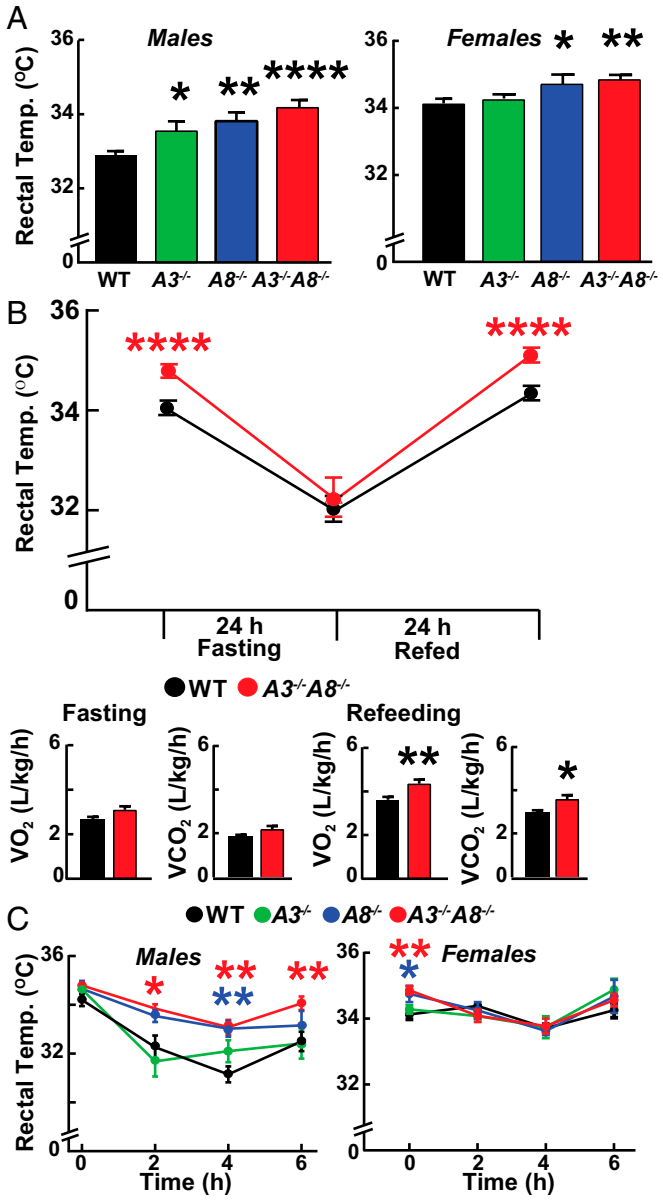

Fig. 2. Rectal temperatures of $A3^{-/-}$, $A8^{-/-}$, $A3^{-/-}A8^{-/-}$, and WT littermates at ambient temperature (21–23 °C) and after exposure to cold (6 °C). (*A*) Rectal temperatures were measured in male (*Left*) and female (*Right*) mice (n = 8–9 per group; age 7–9 wk) fed ad libitum. (*B*) Rectal temperatures (*Upper*) and indirect calorimetry measurements (*Lower*) were obtained in male mice (n = 11 per group, age 6–8 wk) that were fed ad libitum (*Right Lower*) and then after fasting for 24 h. Food was then provided, and the rectal temperature was remeasured at 24 h. VO_2 consumption and CO_2 output measurements were taken during the last 6 h of the fasting and refeeding periods. (*C*) Rectal temperatures were obtained every 2 h in male (*Left*) and female (*Right*) mice maintained for 6 h at 6 °C with free access to food (n = 5 or 6 per group, age 13–15 wk). Values are means ± SEM. Groups were compared by using unpaired t tests. *P < 0.05; **P < 0.01; ****P < 0.0001. The experiments were repeated twice, and the results were similar.

was performed after 24 h. Feeding restored the differences in temperature within 24 h (Fig. 2 *B*, *Lower*).

We measured VO_2 consumption and VCO_2 output during the last 6 h of the fast and again during the last 6 h of the refeeding cycle (Fig. 2 *B*, *Upper*). No differences in VO_2 consumption or VCO_2 output between the groups of mice were seen during the fast, whereas the differences observed in ad libitum-fed animals were apparent at the end of the refeeding period, when A3 and A8 are expressed at the highest levels (6, 7).

No A3 or A8 Detected in the Brain of Mice. *A3* was reported to be expressed in the mediobasal hypothalamus (12), which plays an important role in body temperature regulation and coordination of energy homeostasis (13). To determine the distribution of expression of *A3* and *A8* in the brain, we stained brains of $A3^{-/-}$ and $A8^{-/-}$ mice with X-gal to detect the expression of *LacZ*, which was included in the targeting vector used to generate the KO mice (7, 8). Liver provided a positive control for the expression of A3 and A8. Background staining was apparent in intact liver, but not in sections. As a positive control for detection of LacZ in the brain, we also examined tissue from mice in which *LacZ* was inserted into *Mef2* (14). No LacZ staining was detected in the brains of either the $A3^{-/-}$ or $A8^{-/-}$ mice despite intense staining in the liver (Fig. S4*A*). To confirm these findings, we performed immunohistochemistry on brain slices from both fasted and refed mice using an anti–β-gal antibody. Immunostaining of slices taken through the mediobasal hypothalamus revealed no evidence of *A3* expression (Fig. S4*B*). Immunostaining in sections from cortical tissue of $Mef2^{-/-}$ mice served as a positive control for the experiment. Finally, expression profiling of the hypothalamus from WT mice by using microarrays failed to identify either the A3 or A8 transcript. Whereas we cannot exclude a role for A3 or A8 in CNS-mediated control of metabolism, these data are not consistent with expression of A3 or A8 in the hypothalamus under these conditions.

Preserved Response to Cold Exposure with Reduced Intradermal Fat in $A3^{-/-}A8^{-/-}$ Mice. To determine if the increased body temperature in the $A3^{-/-}A8^{-/-}$ mice was due to a defect in temperature perception, mice were kept at 6 °C for 6 h. In the $A3^{-/-}$ male mice, body temperature dropped significantly after 2 h, but did not decrease further. In the other three groups of male mice, body temperatures continued to fall for the first 4 h (Fig. 2*C*), but did not fall further at the 6-h time point. The reductions in body temperature with cold exposure were not seen in the female mice, as has been reported (15). These data indicate that the $A8^{-/-}$ and $A3^{-/-}A8^{-/-}$ mice defend their body temperatures; therefore, the perception of (and thermogenic response to) cold is preserved in these animals.

To determine if the higher temperatures of the $A3^{-/-}A8^{-/-}$ mice were due to increased insulation, we measured and compared the thickness of the intradermal fat layer between the groups of mice. Hematoxylin/eosin (H&E)-stained sections taken from the midabdomen of mice (n = 3 per group) showed that the amounts of intradermal fat in the male $A3^{-/-}$, $A8^{-/-}$, and WT mice were not significantly different (Fig. S5*A*). Intradermal fat was consistently more plentiful in female than male mice. In the $A3^{-/-}A8^{-/-}$ mice, the intradermal fat layer was almost undetectable in male mice and markedly depleted in female animals. Thus, the increase in body temperature in the $A3^{-/-}A8^{-/-}$ mice, which was maintained in response to a cold challenge, cannot be attributed to increased intradermal fat in these animals.

Beiging and Increased Collagen Content of WAT-SQ from $A3^{-/-}A8^{-/-}$ Mice. The gross appearance and histology of the WAT-Epi and BAT were similar in $A3^{-/-}A8^{-/-}$ and WT mice (Fig. 3 *A*, *Top*). The weights of the WAT-SQ (1.045 ± 0.07 vs. 0.96 ± 0.05 g) and BAT (0.25 ± 0.01 vs. 0.28 ± 0.01 g) did not differ between the two groups. The WAT-Epi was reduced by ∼50% in the double-KO animals (0.92 ± 0.063) compared with the WT mice (1.85 ± 0.13) (P < 0.0001).

On microscopic sectioning, no differences were seen in either the size or morphology of adipocytes in WAT-Epi or BAT (Fig. 3 *A*, *Bottom*). In contrast, the inguinal fat, which is a WAT-SQ depot, was darker in the $A3^{-/-}A8^{-/-}$ than in WT mice, and the

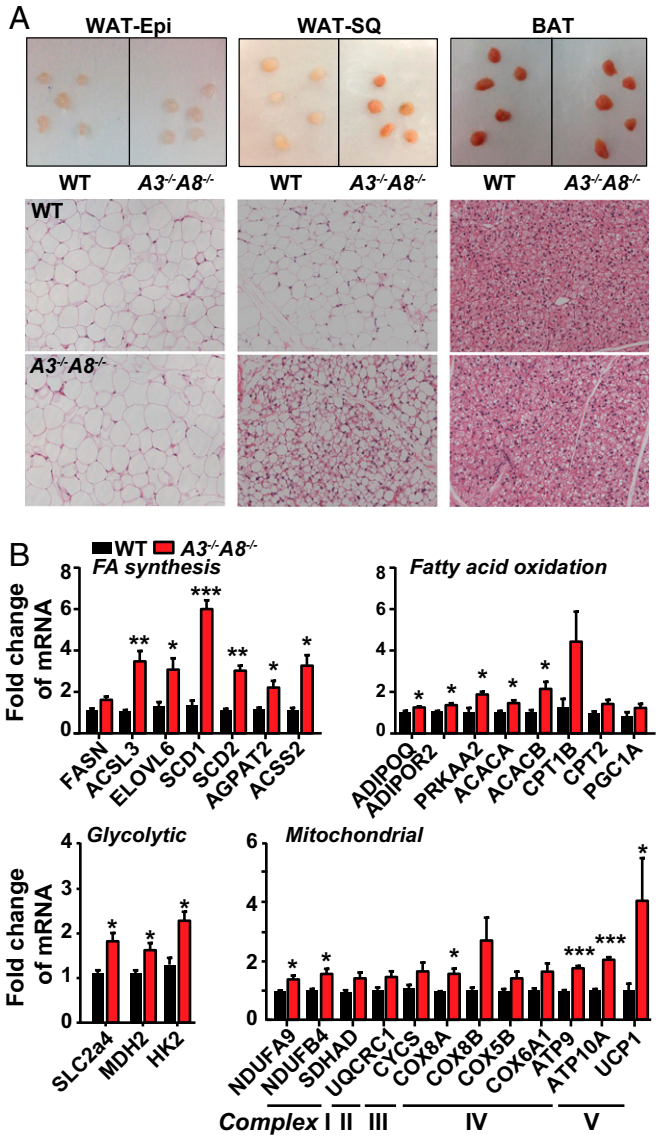

Fig. 3. Adipose tissue morphology and mRNA levels in chow-fed $A3^{-/-}A8^{-/-}$ and WT littermates. (*A*) Representative images of tissue chunks (*Upper*) and H&E staining of adipose tissue sections (*Lower*) ($n = 4$; age 18 wk; three fields per mouse). (Magnification: 20×.) The experiment was repeated twice, and the results were similar. (Scale bars: 50 μm.) (*B*) Fold changes in levels of selected mRNAs encoding proteins involved in fatty synthesis and oxidation (*Upper*) and glycolysis and mitochondrial function (*Lower*) in WAT-SQ of male WT and $A3^{-/-}A8^{-/-}$ mice ($n = 3$ per group; age 18 wk) fasted overnight and then fed for 4 h. Transcript levels were determined by RNA-seq as described in *Materials and Methods*. Values are means ± SEM. Groups were compared using unpaired *t* tests. $*P < 0.05$; $**P < 0.01$; $***P < 0.001$. The experiment was repeated once, and the results were similar.

adipocytes in this depot were significantly smaller in the double-KO mice than in their WT littermates (Fig. 3 *A*, *Middle*).

Picrosirius Red staining of tissue sections from WT and $A3^{-/-}A8^{-/-}$ mice showed an increase in collagen fibers within the extracellular matrix (Fig. S5*B*). This increase was associated with higher levels of mRNAs encoding several collagen genes (Fig. S5*C*). To determine if the increase was a response to inflammation, we compared expression levels of several interleukins and adhesion proteins; the levels of these mRNAs were reduced in the $A3^{-/-}A8^{-/-}$ mice compared with the WT animals, although the differences were not significant (Fig. S5*D*).

Evidence of Up-Regulation of both FA Synthesis and Oxidation in WAT-SQ of $A3^{-/-}A8^{-/-}$ Mice. Previously, we documented a major change in trafficking of FAs from circulating TG in the fed, but not fasted, state in both $A3^{-/-}$ and $A8^{-/-}$ mice (8, 9). Diet-derived FAs are normally routed preferentially to WAT for uptake and storage, but in these two strains of KO animals, FAs from VLDL-TG are cleared from the circulation predominantly by oxidative tissues (8, 9). As a consequence, the usual augmentation in FA delivery to WAT after a meal is abolished, and WAT maintains its mass by increasing the uptake of glucose and converting it to TG (9).

The mRNA expression pattern in the WAT of $A3^{-/-}A8^{-/-}$ mice reflected the expected changes in energy substrate utilization based on the phenotypes of the $A3^{-/-}$ and $A8^{-/-}$ mice. Levels of several mRNAs encoding enzymes involved in FA synthesis were increased (Fig. 3 *B*, *Upper Left*). mRNA levels of enzymes involved in FA oxidation (Fig. 3 *B*, *Upper Right*) and in glycolysis (Fig. 3 *B*, *Lower Left*) were also significantly increased. Expression levels of genes encoding selected mitochondrial proteins, including several components of the electron transport chain, were increased (Fig. 3 *B*, *Lower Right*). UCP1 mRNA expression was much lower in WAT compared with BAT (C_t values from RT-PCR were 23–25 vs. 15–16 in BAT, respectively); levels of this transcript were significantly increased in two experiments ($P = 0.048$) but the mRNA levels were highly variable among animals. Transcripts associated with browning and beiging of fat did not differ significantly between WT and $A3^{-/-}A8^{-/-}$ mice in WAT-SQ, with two exceptions; levels of PPARα and EBF2 were significantly higher in the WAT-SQ of the $A3^{-/-}A8^{-/-}$ mice (Fig. S6*A*). No differences in mRNA levels of enzymes involved in FA synthesis and oxidation were observed in BAT from WT and $A3^{-/-}A8^{-/-}$ mice (Fig. S6*B*). Increased expression of some of the genes involved in glycolysis and mitochondrial function were observed in BAT from the double-KO animals, but no difference in level of UCP1 mRNA was found in BAT of the two strains.

The visible browning of the WAT-SQ (Fig. 3 *A*, *Middle*), together with the increased expression of mitochondrial genes in that tissue, suggested an increase in the number and/or size of the mitochondria in subcutaneous adipose tissue of the $A3^{-/-}A8^{-/-}$ mice.

Increased Size, but Not Number, of Mitochondria in WAT-SQ of $A3^{-/-}A8^{-/-}$ Mice. The ratios of mitochondrial DNA to nuclear DNA in WAT-Epi, WAT-SQ, and BAT were similar in WT and $A3^{-/-}A8^{-/-}$ mice (Fig. 4 *A*, *Left*). Thus, the increase in mRNA levels of mitochondrial genes in the WAT-SQ (Fig. 3*B*) was not due to an increase in the number of mitochondria per adipocyte. Similarly, no significant differences were seen in the protein content of the mitochondrial fraction (per gram of tissue) isolated from WAT-Epi and BAT (Fig. 4 *A*, *Right*). In contrast, the protein content of the mitochondrial fraction was higher in the WAT-SQ of the $A3^{-/-}A8^{-/-}$ mice. The morphology of the mitochondria was examined by electron microscopy (EM) and was consistent with these findings. The mitochondria of the $A3^{-/-}A8^{-/-}$ mice were larger in WAT-SQ (Fig. 4*B*), but not in WAT-Epi or BAT, than those of WT animals (Fig. S7 *A* and *B*). These results suggest that the increase in body temperature in the $A3^{-/-}A8^{-/-}$ mice may be due to metabolic dysregulation that results in simultaneous increases in FA synthesis and FA oxidation in WAT. If this were the case, then energy consumption in the WAT-SQ should be increased in the double-KO animals, especially in the fed state.

Increased O_2 Consumption in WAT-SQ from $A3^{-/-}A8^{-/-}$ Mice in the Fed, but Not Fasted, State. To assess mitochondrial function, we used a Seahorse XF Analyzer to measure the O_2 consumption rates (OCRs) of adipose tissue explants from the three fat depots (Fig. S7*C*), as described in *Materials and Methods*. In six independent experiments performed in fed animals, the OCR was significantly higher in WAT-SQ from $A3^{-/-}A8^{-/-}$ mice than from

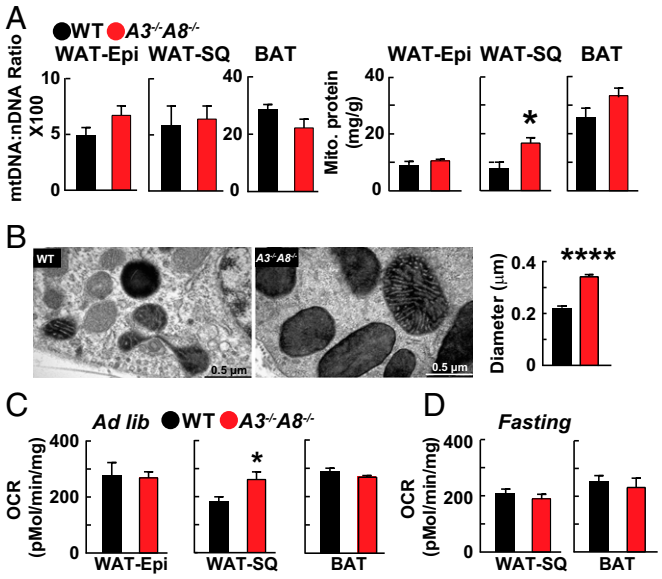

Fig. 4. Mitochondrial number, protein content, and size in WAT-SQ from $A3^{-/-}A8^{-/-}$ and WT mice. (*A*) Ratio of mitochondrial to nuclear DNA (*Left*) and mitochondrial protein content (*Right*) of WAT-Epi, WAT-SQ, and BAT was determined by using mitochondria isolated by centrifugation. The amount of protein was normalized by tissue sample weight ($n = 6$ mice per group; age 11–13 wk). (*B*) Electron micrographs (*Left*) and mean (±SE) diameter (*Right*) of the mitochondria from WAT-SQ. (Scale bars: 0.5 μm.) (*C* and *D*) A Seahorse XF24 analyzer was used to measure extracellular OCRs in adipose tissue in mice fed a chow diet ad libitum (*C*) and after a 14-h fast (*D*) ($n = 6$; with five replicates per mouse). Values are means ± SEM. Groups were compared by using unpaired *t* tests. $^{*}P < 0.05$; $^{****}P < 0.00001$.

their WT littermates (Fig. 4*C*). In contrast, no differences in OCR were detected in WAT-Epi or BAT between the two groups of mice. Since the effects of A3 and A8 on tissue uptake of circulating TG (8, 9) and body temperature (Fig. 2*B*) were only evident in fed animals, we examined the effects of food intake on OCR in the WAT-SQ of the $A3^{-/-}A8^{-/-}$ and WT mice. The increase in OCR observed in explants from fed animals was abolished in WAT-SQ tissue taken from animals that had been fasted for 14 h (Fig. 4*D*). Thus, the increase in VO_2, body temperature, and OCR of WAT-SQ in $A3^{-/-}A8^{-/-}$ mice was only observed in the fed state, a time when A3 and A8 are expressed at highest levels (8, 9).

Elevated Rectal Temperatures of $A3^{-/-}A8^{-/-}$ Mice Were Abolished at Thermoneutrality. To determine if the increase in body temperature in the $A3^{-/-}A8^{-/-}$ mice persists at thermoneutrality, we kept the mice at 30 °C for 5 wk. At the end of the experiment, the rectal temperatures and VO_2 consumption of the $A3^{-/-}A8^{-/-}$ mice did not differ from those of WT animals (Fig. 5*A*), although the body weights of the $A3^{-/-}A8^{-/-}$ male mice remained lower than those of WT mice. No differences in any of these parameters were seen in female mice (Fig. S8). Thus, the thermogenic effect of coinactivating A3 and A8 was only apparent when the mice were housed at the usual vivarium temperature, which is below the thermoneutral zone (16). This result suggested that sympathetic stimulation, which occurs in response to cold (17), may be required to elicit the hyperthermia associated with inactivation of both A3 and A8.

Blockade of β3-ARs Abolishes the Increase in Body Temperature of the $A3^{-/-}A8^{-/-}$ Mice. Adrenergic stimulation is the primary driver of beige adipose tissue formation and activation (18). To determine if adrenergic stimulation contributes to the increased body temperature of $A3^{-/-}A8^{-/-}$ mice, we treated WT and KO mice with propranolol, a nonselective β-AR blocker (Fig. 5*B*). In this experiment, the mice were either maintained on an ad libitum diet or fasted for 14 h. The mice were then injected with

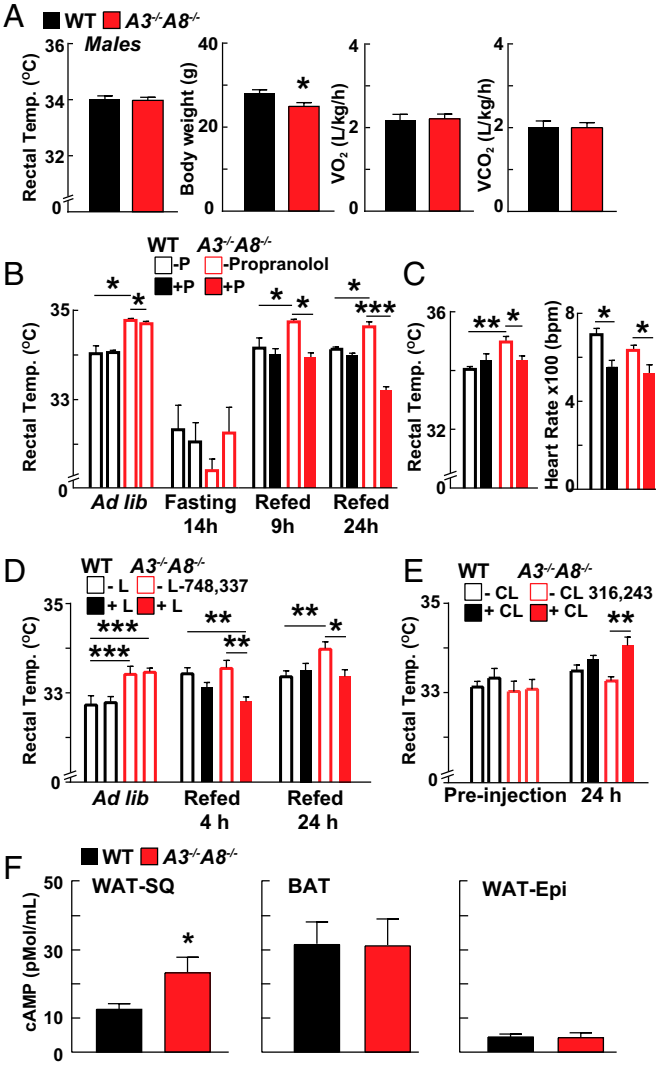

Fig. 5. Effect of thermoneutrality and β-AR blockade on rectal temperature in $A3^{-/-}A8^{-/-}$ and WT chow-fed mice. (*A*) Six-week-old male $A3^{-/-}A8^{-/-}$ and WT mice ($n = 8$ per group) were maintained at thermoneutrality for 5 wk. Rectal temperatures, body weights, VO_2 consumption, and VCO_2 output were measured as described in the *Materials and Methods*. (*B*) Rectal temperatures were obtained in mice fed ad libitum (first 4 bars) or after a 14-h fast (second 4 bars) ($n = 6$; age 9–12 wk). The mice were then treated with a nonselective β-adrenergic blocker (propranolol; 5 mg/kg) and provided food. Temperatures were monitored as described in *Materials and Methods*. (*C*) Male mice ($n = 5$ per group) were treated chronically with propranolol (0.5 mg/mL in the drinking water) starting at 6 wk of age for 5 wk. Heart rates were measured as a control for propranolol activity. (*D*) Mice ($n = 5$ per group; age 7–9 wk) were treated with L-748,337 compound, a β3-receptor blocker (5 mg/kg). (*E*) Male mice were maintained at thermoneutrality for 5 wk and then injected twice with CL 316,243 (1 mg/kg, 18 h apart) ($n = 4$; age 16–17 wk). Values are means ± SEM. Group means were compared by using unpaired *t* tests. Experiments were repeated once, and the results were similar. (*F*) cAMP levels were measured in tissue lysates from WAT-SQ, BAT, and WAT-Epi of WT and $A3^{-/-}A8^{-/-}$ mice fed ad libitum ($n = 5$; age 8–11 wk). Levels were measured by using an ELISA, as described in *Materials and Methods*. Values are means ± SEM. Groups were compared by using unpaired *t* tests. Experiments were repeated once, and the results were similar. CL, CL 316,243; L, L-748,337; P, propranolol. $^{*}P < 0.05$; $^{**}P < 0.01$; $^{***}P < 0.001$.

propranolol or saline solution and given free access to food. At baseline, $A3^{-/-}A8^{-/-}$ mice had higher temperatures when provided food ad libitum (Fig. 5 *B*, *Left*). Fasting reduced the temperatures of the both groups of mice, so at the time of propranolol administration (14 h after food withdrawal), rectal temperatures were similar in the WT and KO groups. Propranolol did not affect the body temperatures of WT mice after refeeding. The temperatures of propranolol-treated $A3^{-/-}A8^{-/-}$ mice were indistinguishable from the WT mice at the 9-h time point and lower than the WT mice at the 24-h time point (Fig. 5*B*).

To ensure that the effects of β-AR blockade on body temperature persisted over time, the mice were treated chronically with propranolol for 5 wk (Fig. 5*C*). Chronic β-AR blockade normalized the body temperature of the $A3^{-/-}A8^{-/-}$ mice. Heart rates of the animals were monitored to ensure that both groups of mice obtained similar amounts of the drug. The decreases in heart rates were comparable in WT and double-KO mice (Fig. 5*C*).

Pharmacological Antagonism of β3-AR with L-748,337. Sympathetic activity in WAT is mediated primarily by the β3-AR (19). Therefore, we repeated the acute β-blockade experiment using a specific β3-AR antagonist, L-748,337. As noted above, the temperatures of the KO mice were higher than those of WT mice on an ad libitum diet (Fig. 5*D*, first 4 lanes). L-748,337 (5 mg/kg) was then given i.p. to the mice (Fig. 5*D*). Treatment was not associated with any differences in rectal temperature in the WT mice at either the 4- or 24-h time point. In contrast, in the $A3^{-/-}A8^{-/-}$ mice, L-748,337 treatment caused a significant reduction in body temperature at both the 4- and 24-h time points. At the 24-h time point, the temperatures of the L-748,337–treated $A3^{-/-}A8^{-/-}$ and saline-treated WT mice were not significantly different.

The results of these experiments were consistent with the notion that the increased body temperatures in the $A3^{-/-}A8^{-/-}$ mice are caused by increased β3-AR signaling in WAT-SQ. If this explanation is correct, then treatment of WT and $A3^{-/-}A8^{-/-}$ mice at thermoneutrality with a β3-AR agonist should result in an increase in rectal temperature only in the KO animals. Consistent with our prior findings (Fig. 5*A*), the rectal temperatures of KO and WT mice kept at thermoneutrality were similar before administration of the β3-AR agonist CL 316,243 (1 mg/kg) (Fig. 5*E*, first 4 lanes). Treatment with the agonist caused an increase in rectal temperature in the KO mice, but not in the WT animals (Fig. 5*E*). From these experiments, we concluded that the increase in body temperature in the $A3^{-/-}A8^{-/-}$ mice was due to an increase in sensitivity of WAT-SQ to the β3-AR agonist.

To test this possibility, we compared cAMP levels in adipose tissue depots of WT and $A3^{-/-}A8^{-/-}$ mice. cAMP levels were significantly increased in the WAT-SQ, but not in WAT-Epi or BAT, of the $A3^{-/-}A8^{-/-}$ mice compared with WT controls (Fig. 5*F*).

Next, we asked if the metabolic changes observed in the $A3^{-/-}A8^{-/-}$ mice could be replicated by blocking the effects of circulating A3 and A8.

Acute Inactivation of A3 and A8 Together, but Not Alone, Increased Temperature in $A3^{-/-}A8^{-/-}$ Mice. Acute inactivation of A3 and A8 by using monoclonal antibodies decreases circulating lipoprotein levels within 1 h of administration (20, 21). To determine the time course of the metabolic changes associated with deficiency of A3 and A8, we administered antibodies against the two proteins either singly or together to mice in which endogenous *A8* was replaced with the human homolog (21). This was required since we do not have an inactivating antibody to mouse A8. The body temperatures of mice injected with either anti-A3 or -A8 alone were not significantly altered. In contrast, when both antibodies were administered to the mice, body temperatures increased significantly within 48 h after the injection (Fig. 6*A*).

Discussion

The major finding of this study is that energy homeostasis is markedly altered in mice lacking both A3 and A8. Targeted inactivation of both genes was associated with increases in body temperature and metabolic rates and with decreases in fat mass and beiging of WAT-SQ (Figs. 1*B* and 3*A*). The hypermetabolic features of the $A3^{-/-}A8^{-/-}$ mice, including hyperthermia and increased VO_2 consumption and VCO_2 output, were most pronounced in fed animals, and were markedly attenuated with fasting (Fig. 2*B*). Consistent with these findings, OCRs were elevated in explants of WAT-SQ taken from fed, but not fasted, $A3^{-/-}A8^{-/-}$ mice (Fig. 4*D*). No changes in OCR were observed in

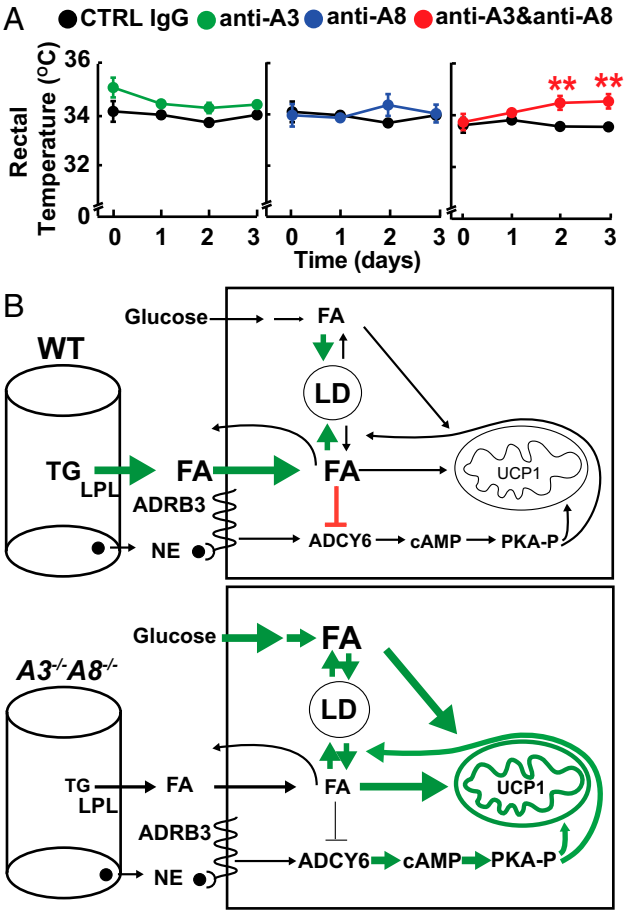

Fig. 6. Effect of inactivating circulating A3, A8, and A3 plus A8 on rectal temperature. (*A*) Anti-human A8 (REGN3776; 10 mg/kg) and anti-mouse A3 (REGN1500; 10 mg/kg) or control monoclonal antibodies (CTRL IgG; RG1945) were given i.v. for 3 d to $ANGPTL8^{hum/hum}$ mice ($n = 6$ per group; age 9 wk). Values are means ± SEM. Groups were compared by using unpaired *t* tests. $^{**}P < 0.01$. The experiment was repeated, and the results were similar. (*B*) Overview of postprandial TG metabolism in WAT-SQ from WT (*Upper*) and $A3^{-/-}A8^{-/-}$ (*Lower*) mice. In fed WT mice, circulating dietary TGs are hydrolyzed by LPL, and FAs are taken up into adipocytes, where they are esterified and stored as TG in lipid droplets. Norepinephrine (NE) activates β3-AR, resulting in activation of ADCY6, which generates cAMP and subsequent phosphorylation and activation of protein kinase A (PKA-P). PKA-P activates both TG hydrolysis and oxidative phosphorylation; the rise in intracellular FA inhibits ADCY6, thus inhibiting these downstream pathways. In WAT-SQ from $A3^{-/-}A8^{-/-}$ mice, LPL in oxidative tissues fails to be suppressed, resulting in diminished delivery of circulating TG to WAT (9). Glucose uptake and its conversion to FAs is increased in these animals. The reduced intracellular concentration of FA may fail to suppress ADCY6, accounting for the increased in cAMP levels. We hypothesize that this results in activation of PKA, causing an increase in both lipolysis and oxidative phosphorylation.

WAT-Epi or BAT in either the fed or fasted state. The hyperthermic response to feeding was blocked by administration of a β3-AR antagonist (Fig. 5*D*) or by maintaining mice at a thermoneutral temperature (Fig. 5*A*). At thermoneutrality, treatment with a β3-AR agonist restored the hyperthermia in the $A3^{-/-}A8^{-/-}$ mice (Fig. 5*E*). Antibody-mediated inactivation of circulating A3 and A8 recapitulated the hyperthermia seen in the $A3^{-/-}A8^{-/-}$ mice (Fig. 6*A*). Together with our prior findings (7, 8), these data indicate that coordinated action of circulating A3 and A8 contributes to efficient postprandial energy utilization by ensuring appropriate partitioning of energy substrates between oxidative tissues and WAT and by attenuating the increase in energy consumption associated with food intake (22).

The diminished accretion of fat observed in $A8^{-/-}$ mice (Fig. 1*B*) is consistent with our prior observations in these animals (8). Our initial hypothesis was that the reduction in fat mass was a direct consequence of decreased uptake of FA from circulating TG, but this notion was dispelled by finding that $A3^{-/-}$ mice, which have a similar defect in TG uptake by WAT, do not have reduced body fat (7). Therefore, the decrease in TG accumulation by WAT of $A8^{-/-}$ mice is not due simply to a failure to replenish TG stores in WAT that are depleted during fasting. The major morphological and metabolic changes associated with inactivation of A3 and A8 occurred primarily in WAT-SQ, and yet the mass of this depot was preserved in the $A3^{-/-}A8^{-/-}$ animals. In contrast, WAT-Epi mass was decreased by ∼50%, despite no increase in OCR or cAMP levels in this tissue. The reduction in WAT-Epi mass without a concomitant reduction in cell size indicates a reduction in the number of WAT-Epi adipocytes in these animals. The mechanism responsible for the decreased number of adipocytes in WAT-Epi is currently unknown.

Nor does the reduction in WAT mass in $A8^{-/-}$ and $A3^{-/-}A8^{-/-}$ mice appear to be developmental, since it was not apparent during the first week of life (Fig. S1*A*) and could be elicited in adult mice by antibody-mediated inactivation of A8 (21). Metabolic cage studies indicated that the decrease in fat accumulation associated with inactivation of *A8* was not caused by reduced food intake or increased physical activity (Fig. 1*C*). The increase in VO_2 consumption, without a concomitant increase in physical activity, in the $A8^{-/-}$ mice is consistent with a metabolic increase in energy expenditure.

A striking and distinctive finding of this study was the increase in body temperature in the $A3^{-/-}A8^{-/-}$ male mice (Fig. 2*A*). The single-KO mice also had increased body temperatures, although the increases were not as pronounced as those seen in the double-KO animals. We found no evidence of a defect in temperature sensing in the $A3^{-/-}A8^{-/-}$ mice (Fig. 2*C*). It was previously reported that A3 is expressed in the hypothalamus, which plays an important role in temperature control (13), but we failed to find evidence that either A3 or A8 are expressed in the hypothalamus, or any other region of the central nervous system (Fig. S4). Therefore, we do not think that the hyperthermia in the $A3^{-/-}A8^{-/-}$ mice reflects central effects of A3 or A8 on body temperature.

Nor did we find evidence that the three strains of KO mice had an inability to dissipate heat due to increased insulation. The $A3^{-/-}A8^{-/-}$ mice had a marked reduction in intradermal fat (Fig. S4*A*), a fat depot that responds rapidly to small changes in temperature with significant alterations in its thickness (23). Changes in dermal fat may have substantial effects on heat loss. The best-characterized mouse model of intradermal fat depletion is the syndecan1 KO, which has a marked reduction in intradermal fat and a 1.8-fold increase in heat loss compared with WT animals (24). The increase in energy required to compensate for the heat loss caused by the reduction in intradermal fat in the $A3^{-/-}A8^{-/-}$ mice may account for some of the increase in VO_2 consumption seen in these animals. However, the role of dermal fat in insulation remains controversial (25). Alteration of dermal fat thickness in mice acclimated to different temperatures did not affect insulation (25). Therefore, it appears likely that the reduction in intradermal fat in the $A3^{-/-}A8^{-/-}$ mice is a consequence, rather than a cause, of the hypermetabolism in these animals.

The hyperthermia in the $A3^{-/-}A8^{-/-}$ mice was abolished by blockade of the β3-AR, a receptor that is expressed predominantly in adipose tissue (26). Unless there is aberrant expression of this receptor in another tissue, which we found no evidence to support, WAT-SQ is the major site of increased metabolism in these mice. The inguinal fat pads (WAT-SQ) of $A3^{-/-}A8^{-/-}$ mice were visibly darker than those of WT animals and had several features characteristic of beiging: smaller adipocytes, larger mitochondria, and increased oxidative phosphorylation (11) (Fig. 3). In contrast to WAT-SQ, no differences in morphology, mitochondrial size, or OCR were apparent in WAT-Epi or BAT from $A3^{-/-}A8^{-/-}$ mice compared with WT animals (Fig. 4*C* and Fig. S7). The change in appearance of adipocytes in WAT-SQ of $A3^{-/-}A8^{-/-}$ mice was accompanied by changes in mRNA expression, especially of genes involved in synthesis and oxidation of FAs (Fig. 3*B*). In addition, we showed previously that TG lipolysis in WAT is not fully suppressed with refeeding in $A3^{-/-}$ mice, despite intact insulin signaling in the tissue (9). The paradoxical increase in both FA synthesis and FA oxidation likely contributed to the increased OCR in this fat depot (Fig. 4*C*). Moreover, expression of UCP1, although significantly lower in WAT than in BAT, was increased in WAT-SQ in the $A3^{-/-}A8^{-/-}$ mice (Fig. 3*B*).

The hypermetabolic phenotype of $A3^{-/-}A8^{-/-}$ mice was only seen when they had access to food (Figs. 2*B* and 4*C*). These results are consistent with our prior finding that A3 and A8 act primarily in the postprandial state where it inhibits LPL activity in oxidative tissues (6, 8, 9). The increase in thermogenesis that occurs in response to feeding includes the energetic cost of digesting, absorbing, and storing food (referred to as the thermic effect of food) (27), which is low for fats (0–3%), intermediate for carbohydrates (5–10%), and greatest for proteins (20–25%) (28). The function of A3 and A8 in directing dietary fats to WAT for storage presumably contributes to the low energy cost of fat consumption and utilization. Feeding-associated energy expenditure in excess of the obligate energy cost of processing food has been referred to as diet-induced thermogenesis (29). The thermogenic responses to feeding, like the responses to cold exposure, have been considered to be mediated by β-adrenergic stimulation of uncoupled mitochondrial energy consumption in BAT (29, 30). Nedergaard and coworkers (31, 32) reported that diet-induced thermogenesis is entirely dependent on UCP1 in BAT. The increased thermogenesis observed in mice lacking both A3 and A8 is also mediated by β-adrenergic stimulation, but appears to arise in WAT-SQ rather than BAT. Therefore, the increased thermogenesis in $A3^{-/-}A8^{-/-}$ mice reflects a process that is distinct from what was described by Nedergaard and coworkers (31, 32).

Why is the body temperature of the KO mice increased at ambient temperature and not at thermoneutrality (Fig. 5*A*)? One possibility is that the KO mice have an amplified thermogenic response to cold exposure in WAT-SQ, either due to increased levels of norepinephrine or to increased WAT-SQ responsiveness to the hormone. Consistent with this scenario, administration of a β3-AR antagonist prevented the temperature increase in the KO mice (Fig. 5 *B*–*D*). Conversely, at thermoneutrality, treatment with a β3-AR agonist significantly increased body temperature in $A3^{-/-}A8^{-/-}$ mice, but not WT mice (Fig. 5*E*). The effects of this increased sensitivity are not apparent at thermoneutrality since adrenergic stimulation of WAT-SQ is limited under this condition, whereas at ambient temperatures, adrenergic stimulus is increased. Since equivalent doses of β3-AR agonist elicited a greater thermogenic response in $A3^{-/-}A8^{-/-}$ mice

than in their WT littermates, we infer that inactivation of A3 and A8 results in increased sensitivity of WAT-SQ to the adrenergic stimulus rather than an increase in the amount of signal that reaches the cell.

Our studies have not yet elucidated the specific mechanism(s) by which A3 and A8 attenuate β3-AR stimulation of adipocytes in the fed state. Can the diverse metabolic features of the $A3^{-/-}A8^{-/-}$ mice be explained by the inhibitory effects of A3 and A8 on LPL activity? Adipose-tissue-specific KO of LPL, which would be expected to recapitulate the decrease in LPL-mediated uptake of VLDL-TG observed in the $A3^{-/-}A8^{-/-}$ mice, does not affect WAT mass (33–36). Garcia-Arcos et al. (35) reported that adipose-tissue-specific KO of LPL had no effect on microscopic or macroscopic morphology in WAT, and Bartelt et al. (36) found that uptake of dietary FA by WAT was increased in their animals and that administration of a β3-AR agonist for 7 d did not elicit any beiging response. Therefore, the mice used in those studies did not recapitulate the cardinal features of the $A3^{-/-}A8^{-/-}$ animals.

A working model comparing TG metabolism in WAT-SQ from fed WT and $A3^{-/-}A8^{-/-}$ mice is shown in Fig. 6*B*. In fed WT mice, glucose uptake and de novo lipogenesis are low, whereas uptake of VLDL-FAs is increased eightfold compared with fasting animals (9). The increased uptake of FA would be expected to increase intracellular FA concentrations. Mottillo and Granneman (37) reported that treatments that increase intracellular FA concentrations suppress β-adrenergic signaling in white adipocytes by inhibiting adenylate cyclase (ADCY6), thereby acting as a feedback mechanism to limit lipolysis and promote storage of FA in lipid droplets (Fig. 6 *B*, *Upper*). Based on prior metabolic studies in $A3^{-/-}$ and $A8^{-/-}$ mice (8, 9), we anticipate that the postprandial increase in FA uptake from VLDL into WAT fails to occur in these animals. Failure to increase FA uptake from VLDL-TG would be expected to lower intracellular FA concentrations and impair suppression of ADCY6, which would increase intracellular cAMP and phosphorylation of protein kinase A in response to β-adrenergic signaling. The finding that cAMP concentrations in WAT-SQ were higher in $A3^{-/-}A8^{-/-}$ mice than in WT animals is consistent with this model (Fig. 5*F*). The simultaneous increases in both the synthesis and oxidation of FA may contribute to the excess heat generation.

It appears that A8, which is expressed at high levels in WAT as well as liver (4–6), also has metabolic effects that are independent of A3 (and of TG uptake by WAT), since the $A8^{-/-}$ and $A3^{-/-}A8^{-/-}$ mice have a more pronounced phenotype than do the $A3^{-/-}$ mice (Fig. 2). We speculate that these effects are mediated by differences in cell signaling in WAT. Testing this hypothesis will require the generation and characterization of tissue-specific A8 KO mice.

Materials and Methods

Mice. $A3^{-/-}$ and $A8^{-/-}$ mice were generated by homologous recombination (*SI Materials and Methods*) and back-crossed with C57BL/6J mice to produce N6 mice. The $A3^{-/-}A8^{-/-}$ mice were obtained by crossing the single-KO lines. Humanized A8 mice ($Angptl8^{hum/hum}$ mice) were generated by using VelociGene technology by Regeneron Pharmaceuticals (21) and maintained at our institution. Mice were kept at 21–23 °C on a 12-h dark/light cycle (lights on: 7:00 AM–7:00 PM). For fasting and refeeding experiments, mice were synchronized for 3 d by removing food during the day (7:00 AM–7:00 PM) and providing food at night (7:00 PM–7:00 AM). All protocols were approved by the Institutional Animal Care and Use Committee of the University of Texas Southwestern Medical Center.

Indirect Calorimetry and Body Composition Measurements. Indirect calorimetry (VO_2 consumption and VCO_2 output), food intake, and physical activity were monitored for 1 min every 30 min for four consecutive days in metabolic cages (LabMaster System; TSE Systems). For measurements of energy homeostasis, mice were acclimated to the new environment for 3 d before data collection. In some experiments, lean mass and total fat mass were determined in nonanesthetized mice by NMR (Bruker).

Studies at Thermoneutrality. WT and $A3^{-/-}A8^{-/-}$ littermates were housed together at 30 °C for 5 wk with free access to water and food, and then housed individually for 5 d at 30 °C before body weights and rectal temperatures were obtained. Mice were then housed in a climatic chamber (Phenomaster; TSE Systems GmbH) and maintained at 30 °C (50% humidity) with a 12-h light/dark cycle (lights on: 7:00 AM–7:00 PM). Indirect calorimetry was then performed.

Rectal Temperature Measurements and Cold-Exposure Test. To assess cold tolerance, mice were placed at 6 °C at 9:00 AM and provided free access to food and water. Rectal temperatures were recorded every 2 h for a total of 6 h. Body temperatures were measured rectally by the insertion by at least 1.5 cm of a thermocouple thermometer probe (BAT-7001H; Physitemp Instrument Inc.).

Histology. Tissues were fixed with paraformaldehyde (4%) overnight, washed with PBS, and then processed for paraffin embedding. Tissues were then sectioned to a thickness of 5 μm and stained with H&E or Picrosirius Red by using standard procedures. Skin samples (1 cm^2) were collected from the medial abdomen and processed for H&E staining. Stained sections were examined by light microscopy (20×), and the thickness of the intradermal fat layer was measured directly on the resulting images. For each mouse, the thickness of the intradermal fat layer was measured at three sites in six or seven images. Dermal thickness was expressed as the mean the three measurements for each image.

mRNA Sequencing. Total RNA was prepared from WAT-Epi, WAT-SQ, BAT, and skeletal muscle (n = 3 per genotype) by using RNaeasy Plus Universal (Qiagen). The integrity of the RNA was assessed by electrophoresis using the Agilent Tapestation 4200, and the concentration was measured on a Qubit fluorometer (Invitrogen). Poly-A RNA-sequencing (RNA-seq) libraries were prepared from 4 μg of DNA-free total RNA by using the TruSeq Stranded Total RNA Ribo-Zero kit (Illumina). Poly-A RNA was purified and fragmented before strand-specific cDNA synthesis. cDNAs were then adenylated and ligated to indexed adapters to allow identification of individual samples. After adapter ligation, samples were amplified by PCR, purified with AmpureXP beads, pooled, and sequenced to a depth of 25 million reads per sample on a NextSeq500 (Illumina) by using 75-nucleotide single-end sequencing by synthesis chemistry. Sequence reads were aligned to the mouse transcriptome (mm10) by using TopHat (ccb.jhu.edu/software/tophat/index.shtml). The alignments were processed further by using the Cufflinks package (cole-trapnell-lab.github.io/cufflinks/) to quantify transcript levels and to identify differentially expressed genes. Transcript levels were calculated as fragments per kilobase of exon per million fragments mapped. Mean values were calculated for each transcript, and fold differences between $A3^{-/-}A8^{-/-}$ and WT littermates were determined.

Mitochondrial DNA to Nuclear DNA Ratio. Total DNA was extracted from WAT-Epi, WAT-SQ, and BAT of six mice of each genotype by using a DNeasy kit (Qiagen). Mitochondrial DNA content was calculated by using quantitative real-time PCR by measuring the threshold cycle ratio (ΔC_t) of a mitochondria-encoded gene, cytochrome *c* oxidase subunit 2 (Cox2) relative to a nuclear-encoded gene, beta adult major chain hemoglobin (Hbb-b1). The PCR primers used for amplification were as follows: Cox2: forward (F), 5′-GCCGACTAAATCAAGCAACA-3′; reverse (R), 5′-CAATGGGCATAAAGCTATGG-3′; and HBB-B1: F, 5′-GAAGCGATTCTAGGGAGCAG-3′; and R, 5′-GGAGCAGCGATTCTGAGTAGA3′.

The threshold cycle number (Ct) values of the nuclear and the mitochondrial genes were determined for each mouse, and data were expressed as mean (±SE) mitochondrial to nuclear DNA ratio.

Isolation of Crude Mitochondria. Tissues were collected, homogenized in 10 volumes of SET buffer (250 mM sucrose, 1 mM EDTA, and 10 mM Tris·HCl, pH 7.4) by using a glass–glass homogenizer, and centrifuged at 450 × *g* for 10 min, all at 4 °C. Pellets were discarded and supernatants centrifuged at 8,000 × *g* for 15 min at 4 °C. The pellet, which contained crude mitochondria, was resuspended in SET buffer (100 μL), and the protein concentration was measured (38). The mitochondrial protein content was normalized to tissue weight.

Transmission EM. For ultrastructural analysis of mitochondria, mice were anesthetized with isoflurane and perfused via the left ventricle with normal saline followed by 3% glutaraldehyde buffered with 0.1 M sodium cacodylate

(pH 7.4). Following perfusion, WAT-Epi, WAT-SQ, and BAT were removed and dissected into small pieces, which were placed in fresh fixative at room temperature for 2 h. Following fixation, tissues were washed overnight in cacodylate buffer at 4 °C and then sequentially treated with OsO4 (1%), tannic acid (2%) (both in PBS), and uranyl acetate (2%) (in distilled water). Tissues were dehydrated by incubation in ethanol (a graded series from 10 to 100%) for 15–30 min at each concentration, followed by incubation in ethanol:propylene oxide (50:50). Tissues were then embedded in Epon and sectioned for transmission EM (TEM). Thin sections (60 nm) were cut, mounted on 200-mesh grids, counterstained with uranyl acetate and lead citrate, and examined by TEM (JEOL 1200EX TEM) at 120 kV. Images were digitally captured. An average of 400 mitochondria per tissue sample were visualized, measured, and sorted by diameter.

OCR by Explants of Adipose Tissue. O_2 consumption by explants from WAT and BAT were measured by using a Seahorse XF Extracellular Flux Analysis. An XF24 FluxPak (catalog no. 101174-100; Seahorse Bioscience) was hydrated by adding XF Calibrant (1 mL) and stored for at least 12 h at 37 °C without CO_2. The day of the experiment, mice were fed ad libitum or fasted for 14 h before being anesthetized using isoflurane and then exsanguinated. WAT-SQ, WAT-Epi, and BAT were excised and placed in fresh Rinse Medium [XF Base Medium (catalog no. 102353-100; Seahorse Bioscience) supplemented with 1 mM sodium pyruvate, 2 mM GlutaMAX-1, 25 mM glucose, and 25 mM Hepes] that had been warmed to 37 °C. Tissues were rinsed and minced into 5- to 10-mg pieces. Each piece was placed in a well of an XF24 Islet Capture Microplate and covered by a screen. Wells were rinsed three times with Rinse Medium and then once with Running Buffer (Rinse Medium minus Hepes). A total of 675 μL of Running Medium was added to each well, and the plate was maintained at 37 °C without CO_2. Basal OCR was obtained in five measurements over a 30-min period, where the medium was mixed (2.5 min) and allowed to stay still (2 min), and then measurements were taken (3 min). Measurements were normalized to tissue weight. Subsequently, three mitochondrial effectors were added to the medium in a serial fashion: oligomycin (2 μM), carbonyl cyanide p-trifluoromethoxyphenylhydrazone (FCCP) (8 μM), and rotenone (3 μM) (Sigma), as described (39). The amount and duration of the incubations was determined for each inhibitor. After addition of oligomycin, five measurements were obtained. For each measurement, the inhibitor was mixed with the sample (3.5 min) and allowed to incubate (2.5 min), and then measurements were taken (4 min). Afterward, FCCP was added, and four measurements were obtained as follows: mix for 3 min, wait for 2 min, and measure over 3 min. Finally, rotenone was added, and eight measurements were obtained. For each measurement, the inhibitor was mixed with the sample (3.5 min) and allowed to incubate (2 min), and then measurements were taken (4 min). Measures were made by using the Seahorse XF24 software and expressed as picomoles per minute.

Administration of Antibodies. Fully human anti-A8 (REGN3776) (21) and anti-A3 (REGN1500) monoclonal antibodies were derived by using Regeneron's VelocImmune technology platform (20). Antibodies were diluted in PBS and administered to mice (10 mg/kg) by tail vein injection. An isotype-matched antibody with irrelevant specificity was used as control (REGN1945). REGN3776 has high affinity for monkey and human A8, but not for mouse A8 (21). Therefore, experiments with REGN3776 were performed in mice expressing human A8.

Administration of β-AR Antagonists. Mice maintained at room temperature were fasted for 14 h. Temperatures were taken by using a rectal probe, and each mouse was given a single i.p. injection of propranolol hydrochloride (catalog no. P0884; Sigma) (5 mg/kg) or L-748,337 (catalog no. 2760; R&D Systems) (5 mg/kg). Mice were fed a chow diet ad libitum, and temperatures were measured after 9 and 24 h (propranolol) and after 4 and 24 h (L-748,337). In a second experiment, mice that were maintained at 30 °C were treated with CL 316,243 (catalog no. C5976; 1 mg/kg mouse; Sigma) by i.p. injection. Each mouse received two injections, 18 h apart. In a third experiment, WT and $A3^{-/-}A8^{-/-}$ mice were given propranolol (0.5 mg/mL) in the drinking water for 5 wk. Water bottles were replaced with freshly made supplemented water every 3 d.

Heart rates of WT and $A3^{-/-}A8^{-/-}$ littermates that were maintained on propranolol for 5 wk were measured by using the BP-2000 Blood Pressure Analysis System Four-Channel Mouse System (Visitech Systems). Measurements were taken at 11 AM for five consecutive days.

cAMP Assay. Adipose tissue samples were collected at 11 AM from WT and $A3^{-/-}A8^{-/-}$ mice littermates that were fed ad libitum (n = 5 per group). cAMP levels were measured by using a commercial ELISA kit (catalog no. ADI-900-163; Enzo Life Sciences) on tissue lysates as described by the manufacturer. Data were normalized by tissue weights and expressed as picomoles per milliliter.

Statistical Analysis. Total VO_2 consumption and VCO_2 output (per animal) were compared between genotypes by using analysis of covariance (ANCOVA), including body weight as a covariate (40). All other comparisons were performed by using unpaired t tests.

ACKNOWLEDGMENTS. We thank Christina Zhao, Liangcai Nie, and Stephanie Spaeth for excellent technical assistance; Joel Elmquist for providing the mRNA expression profiling data for the brain; Charlotte Lee in his laboratory for assistance with the immunohistochemistry of the hypothalamus; and Syann Lee and Norma Anderson for assistance with the metabolic cage studies. This work was supported by National Institutes of Health Grant 5 P01 HL20948.

1. Kuwajima M, Foster DW, McGarry JD (1988) Regulation of lipoprotein lipase in different rat tissues. *Metabolism* 37:597–601.
2. Kersten S (2014) Physiological regulation of lipoprotein lipase. *Biochim Biophys Acta* 1841:919–933.
3. Kersten S, et al. (2000) Characterization of the fasting-induced adipose factor FIAF, a novel peroxisome proliferator-activated receptor target gene. *J Biol Chem* 275: 28488–28493.
4. Ren G, Kim JY, Smas CM (2012) Identification of RIFL, a novel adipocyte-enriched insulin target gene with a role in lipid metabolism. *Am J Physiol Endocrinol Metab* 303:E334–E351.
5. Zhang R (2012) Lipasin, a novel nutritionally-regulated liver-enriched factor that regulates serum triglyceride levels. *Biochem Biophys Res Commun* 424:786–792.
6. Quagliarini F, et al. (2012) Atypical angiopoietin-like protein that regulates ANGPTL3. *Proc Natl Acad Sci USA* 109:19751–19756.
7. Wang Y, et al. (2015) Inactivation of ANGPTL3 reduces hepatic VLDL-triglyceride secretion. *J Lipid Res* 56:1296–1307.
8. Wang Y, et al. (2013) Mice lacking ANGPTL8 (betatrophin) manifest disrupted triglyceride metabolism without impaired glucose homeostasis. *Proc Natl Acad Sci USA* 110:16109–16114.
9. Wang Y, et al. (2015) Hepatic ANGPTL3 regulates adipose tissue energy homeostasis. *Proc Natl Acad Sci USA* 112:11630–11635.
10. Haller JF, et al. (2017) ANGPTL8 requires ANGPTL3 to inhibit lipoprotein lipase and plasma triglyceride clearance. *J Lipid Res* 58:1166–1173.
11. Kajimura S, Spiegelman BM, Seale P (2015) Brown and beige fat: Physiological roles beyond heat generation. *Cell Metab* 22:546–559.
12. Kim HK, et al. (2015) Regulation of energy balance by the hypothalamic lipoprotein lipase regulator Angptl3. *Diabetes* 64:1142–1153.
13. Blouet C, Ono H, Schwartz GJ (2008) Mediobasal hypothalamic p70 S6 kinase 1 modulates the control of energy homeostasis. *Cell Metab* 8:459–467.
14. Naya FJ, Wu C, Richardson JA, Overbeek P, Olson EN (1999) Transcriptional activity of MEF2 during mouse embryogenesis monitored with a MEF2-dependent transgene. *Development* 126:2045–2052.
15. Harshaw C, Culligan JJ, Alberts JR (2014) Sex differences in thermogenesis structure behavior and contact within huddles of infant mice. *PLoS One* 9:e87405.
16. Cannon B, Nedergaard J (2011) Nonshivering thermogenesis and its adequate measurement in metabolic studies. *J Exp Biol* 214:242–253.
17. Schönbaum E, Johnson GE, Sellers EA, Gill MJ (1966) Adrenergic beta-receptors and non-shivering thermogenesis. *Nature* 210:426.
18. Harms M, Seale P (2013) Brown and beige fat: Development, function and therapeutic potential. *Nat Med* 19:1252–1263.
19. Collins S, et al. (1994) Impaired expression and functional activity of the beta 3- and beta 1-adrenergic receptors in adipose tissue of congenitally obese (C57BL/6J ob/ob) mice. *Mol Endocrinol* 8:518–527.
20. Gusarova V, et al. (2015) ANGPTL3 blockade with a human monoclonal antibody reduces plasma lipids in dyslipidemic mice and monkeys. *J Lipid Res* 56:1308–1317.
21. Gusarova V, et al. (2017) ANGPTL8 blockade with a monoclonal antibody promotes triglyceride clearance, energy expenditure, and weight loss in mice. *Endocrinology* 158:1252–1259.
22. Pittet P, Gygax PH, Jéquier E (1974) Thermic effect of glucose and amino acids in man studied by direct and indirect calorimetry. *Br J Nutr* 31:343–349.
23. Kruglikov IL, Scherer PE (2016) Dermal adipocytes: From irrelevance to metabolic targets? *Trends Endocrinol Metab* 27:1–10.
24. Kasza I, et al. (2014) Syndecan-1 is required to maintain intradermal fat and prevent cold stress. *PLoS Genet* 10:e1004514.
25. Fischer AW, Csikasz RI, von Essen G, Cannon B, Nedergaard J (2016) No insulating effect of obesity. *Am J Physiol Endocrinol Metab* 311:E202–E213.
26. Nahmias C, et al. (1991) Molecular characterization of the mouse beta 3-adrenergic receptor: Relationship with the atypical receptor of adipocytes. *EMBO J* 10: 3721–3727.
27. de Jonge L, Bray GA (1997) The thermic effect of food and obesity: A critical review. *Obes Res* 5:622–631.
28. Nair KS, Halliday D, Garrow JS (1983) Thermic response to isoenergetic protein, carbohydrate or fat meals in lean and obese subjects. *Clin Sci (Lond)* 65:307–312.

29. Rothwell NJ, Stock MJ (1979) A role for brown adipose tissue in diet-induced thermogenesis. *Nature* 281:31–35.
30. Acheson KJ, Ravussin E, Wahren J, Jéquier E (1984) Thermic effect of glucose in man. Obligatory and facultative thermogenesis. *J Clin Invest* 74:1572–1580.
31. Feldmann HM, Golozoubova V, Cannon B, Nedergaard J (2009) UCP1 ablation induces obesity and abolishes diet-induced thermogenesis in mice exempt from thermal stress by living at thermoneutrality. *Cell Metab* 9:203–209.
32. von Essen G, Lindsund E, Cannon B, Nedergaard J (2017) Adaptive facultative diet-induced thermogenesis in wild-type but not in UCP1-ablated mice. *Am J Physiol Endocrinol Metab* 313:E515–E527.
33. Weinstock PH, et al. (1997) Lipoprotein lipase controls fatty acid entry into adipose tissue, but fat mass is preserved by endogenous synthesis in mice deficient in adipose tissue lipoprotein lipase. *Proc Natl Acad Sci USA* 94:10261–10266.
34. Kratky D, et al. (2005) Endothelial lipase provides an alternative pathway for FFA uptake in lipoprotein lipase-deficient mouse adipose tissue. *J Clin Invest* 115:161–167.
35. Garcia-Arcos I, et al. (2013) Adipose-specific lipoprotein lipase deficiency more profoundly affects brown than white fat biology. *J Biol Chem* 288:14046–14058.
36. Bartelt A, et al. (2013) Effects of adipocyte lipoprotein lipase on de novo lipogenesis and white adipose tissue browning. *Biochim Biophys Acta* 1831:934–942.
37. Mottillo EP, Granneman JG (2011) Intracellular fatty acids suppress β-adrenergic induction of PKA-targeted gene expression in white adipocytes. *Am J Physiol Endocrinol Metab* 301:E122–E131.
38. Bradford MM (1976) A rapid and sensitive method for the quantitation of microgram quantities of protein utilizing the principle of protein-dye binding. *Anal Biochem* 72: 248–254.
39. Bugge A, Dib L, Collins S (2014) Measuring respiratory activity of adipocytes and adipose tissues in real time. *Methods Enzymol* 538:233–247.
40. Tschöp MH, et al. (2011) A guide to analysis of mouse energy metabolism. *Nat Methods* 9:57–63.